SEMARAK ILMU PUBLISHING

Journal of Advanced Research in Fluid Mechanics and Thermal Sciences

Journal homepage:
https://semarakilmu.com.my/journals/index.php/fluid_mechanics_thermal_sciences/index
ISSN: 2289-7879

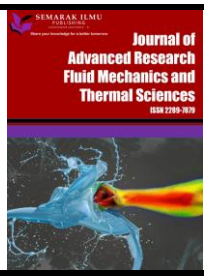

Simulation-Based Radiation Shielding and Optical Properties of Thulium-Doped Bismuth Tellurite Glass

Nur Arina Mat Rusni[1,2], Azuraida Amat[2,*], Wan Yusmawati Wan Yusoff[2], Nor Azlian Abdul-Manaff[2], Nurazlin Ahmad[2], Hasnimulyati Laoding[3], Hiroyo Segawa[4]

[1] Faculty of Defence Science and Technology, National Defense University of Malaysia, Kem Sungai Besi, 57000 Kuala Lumpur, Malaysia
[2] Physics Department, Centre for Defence Foundation Studies, National Defense University of Malaysia, Kem Sungai Besi, 57000 Kuala Lumpur, Malaysia
[3] Physics Department, Faculty of Applied Sciences, Universiti Teknologi MARA Cawangan Pahang, Kampus Jengka, 26400 Jengka, Pahang, Malaysia
[4] National Institute for Materials Science, 1-1 Namiki, Tsukuba 305-0044, Ibaraki, Japan

ARTICLE INFO

Article history:
Received 18 August 2024
Received in revised form 12 November 2024
Accepted 24 November 2024
Available online 10 December 2024

Keywords:
Thulium doped bismuth tellurite; structural properties; radiation shielding properties; optical properties; lead-free glass

ABSTRACT

Lead-based radiation shielding material is currently used in industry to shield against high-penetration radiation such as gamma rays. However, lead is harmful to humans, animals, and plants. This study proposed a new composition of transparent lead-free glass. Using the melt and quench technique, thulium-doped bismuth tellurite glass with composition $(TeO_2)_{1-x}$ $(Bi_2O_3)_x$ $(Tm_2O_3)_{0.02}$ where x = 0.05, 0.10, 0.15, and 0.20 mol % was fabricated. Significantly, the glasses with Bi_2O_3 concentration of 5 mol % and 10 mol% have a higher density than the commercial glass containing lead indicating the fabricated glasses would perform better as a radiation shielding material. Comparing the simulated-radiation shielding properties using software Phy-X and XCom, the glass with 10 mol% of Bi_2O_3 performs better as radiation shielding material than 5 mol% of Bi_2O_3. Meanwhile, glass with 5 mol% of Bi_2O_3 performs better than 10 mol% of Bi_2O_3 in terms of optical properties. Considering both radiation shielding and optical properties, the fabricated lead-free glass can be widely used in radiation shielding applications that require transparency.

1. Introduction

Currently, transparent radiation shielding glass is used in the medical industry as viewing windows to protect healthcare personnel during radiation treatment. However, like a double-edged sword, current radiation shielding glass used in industry contains lead which poses hazardous effects on humans, animals, and plants [1-5]. With the toxicity of lead, alternative development of lead-free radiation shielding glass became crucial. Despite numerous research efforts to develop lead-free glass, it is not easy to compose a glass composition that has high density and clear transparency that

* *Corresponding author.*
E-mail address: azuraida@upnm.edu.my

https://doi.org/10.37934/arfmts.125.1.112126

is at par with lead glass [6-9]. Therefore, a new composition of lead-free radiation shielding glass was proposed.

The chemical compounds of tellurium dioxide (TeO_2), bismuth trioxide (Bi_2O_3), and thulium (III) oxide (Tm_2O_3) were incorporated into the glass composition. Tellurite-based glass is chosen as the glass base mainly due to its high density. TeO_2 has a higher density of 5.67 g/cm^3 compared to commercially used silicon dioxide (SiO_2) with a density of 2.65 g/cm^3. This high density indicates that there is a high potential to be applied as a radiation shielding material since there will be a higher probability of interaction between atoms and harmful radiation such as gamma rays. The interaction of atoms could be either photoelectric effects, pair-productions, or Compton scatterings [10]. Previous studies have shown that glasses with a high density resulted in a high mass attenuation coefficient [11,12]. The mass attenuation coefficient expresses how many photons a homogeneous absorber removes per unit mass from a radiation beam such as x-rays or gamma rays. Apart from that, TeO_2 glasses have a low melting temperature making them a good eco-friendly alternative due to their low energy consumption during the melting process [13]. Also, TeO_2 glasses are transparent in the near UV to mid-IR wavelength range making it suitable to be applied in application that requires the line-of-sight [14]. Then, Bi_2O_3 was incorporated into the glass composition due to its high density and non-toxic to the environment. In wastewater treatment, bismuth nanoparticles have been used to degrade dye, and a toxicology study proved that the treated dye water is non-toxic [15]. In terms of radiation shielding, when bismuth was layered together with a leaded gonad shield, bismuth significantly reduced radiation dose without disrupting the image quality of pelvic X-ray [16]. Hence, this shows the potential of bismuth as a radiation-shielding material. Furthermore, Tm_2O_3 incorporation was found to improve glass structure by improving the connectivity of the glass network and atomic arrangement cross-linkage [17,18]. It was proven that Tm_2O_3 incorporation in the TeO_2 glass system significantly increases the mass attenuation coefficient and linear attenuation coefficient [19,20].

Taking into account the aforementioned considerations, a series of new compositions of tellurite-based glass was fabricated and the optical as well as radiation shielding properties were investigated. The radiation shielding investigation for the mass attenuation coefficient was conducted at a continuous energy range of 0.001 keV to 1000 MeV. Then, further analysis of radiation shielding at energy 0.662 MeV using Cs-137 was conducted. This energy was specifically chosen since the gamma rays with wavelength 0.001874 nm are usually applied in medical procedures such as radiotherapy [21]. Also, a comparison between fabricated glasses with industrial lead glass was made. This study can significantly contribute to the development of lead-free glass that is not only eco-friendly but also can be widely used in transparent radiation shielding applications in the medical industry.

2. Methodology

2.1 Glass Samples Fabrication

New composition of $(TeO_2)_{1-x}$ $(Bi_2O_3)_x$ $(Tm_2O_3)_{0.02}$ where x = 0.05, 0.10, 0.15, 0.20 mol % was fabricated using melt and quench technique. This fabrication technique was chosen due to its simplicity. After stoichiometry calculation, the chemicals of TeO_2, Bi_2O_3 and Tm_2O_3 supplied from Alfa Aesar with 99.99% purity were weighted using a PGW 214 analytical balance from AE Adam. The weighted chemical was then transferred to a natural agate mortar and pestle. To ensure the chemicals were mixed homogenously, the chemicals were grounded for an hour. After grounding, the chemicals were then transferred to an alumina crucible for the preheating process in an electric furnace. After an hour of preheating at 400 °C to eliminate water vapour, the melting process was carried out in a different furnace for an hour at 900 °C. While the melting process occurred, a

stainless-steel mould was heated at 400 °C to avoid thermal shock on the high-temperature molten sample. This thermal shock could cause the glass sample to have a higher susceptibility to crack during the annealing process. Following the melting process, the molten sample was poured onto a heated stainless-steel mould and placed in an electric furnace to undergo an additional 1 hour of annealing at 400 °C. The sample was then allowed to cool to ambient temperature.

2.2 Density and Molar Volume Measurement

The density measurement was conducted using an MGS-300 density meter from Alfa Mirage. Archimedes's principle was applied, and Eq. (1) was used for the calculation of the glass density.

$$\rho_{glass} = \left(\frac{w_{air}}{w_{air} - w_{water}}\right)(\rho_{water}) \tag{1}$$

where the symbol ρ_{glass}, ρ_{water}, w_{air} and w_{water} referred to glass density, water density, glass weight in air and glass weight in distilled water, respectively.

The molar volume (V_m) of fabricated glass was calculated using the Eq. (2).

$$V_m = \left(\frac{M_m}{\rho_{glass}}\right) \tag{2}$$

The symbol M_m in Eq. (2) stands for the relative molar mass of glass samples.

Using the value of V_m, oxygen packing density (OPD) was calculated using Eq. (3) [22].

$$OPD = \frac{1000 \times c}{V_m} \tag{3}$$

where c represent the number of oxygens per unit formula.

2.3 Structural Properties Characterization

Structural characterization was conducted by Fourier Transform Infrared Spectroscopy (FTIR). The FTIR measurement was conducted from 600 cm^{-1} to 4000 cm^{-1} wavenumbers using a Perkin Elmer FT-IR Spectrometer Frontier. FTIR measurement enables the analysis of the network in the glass structure. The examined glasses were in the form of solid glass samples.

2.4 Theoretical Radiation Shielding Properties Measurements

Web-based radiation shielding software Phy-X and XCom were used to measure the radiation shielding parameters such as mass attenuation coefficient (MAC), half-value layer (HVL), and mean free path (MFP) of glass samples. For software Phy-X, the radiation shielding parameters were obtained directly from the software. However, for software XCom, radiation shielding parameters such as HVL and MFP were obtained through manual calculation since only MAC value can be obtained directly from the software. Using the value of linear attenuation coefficient (LAC) as shown in Eq. (4), the value of HVL and MFP were calculated using Eq. (5) and Eq. (6), respectively.

$$LAC = MAC \cdot \rho_{glass} \tag{4}$$

$$HVL = \frac{In\,(2)}{LAC} = \frac{0.693}{LAC} \tag{5}$$

$$MFP = \frac{1}{LAC} \tag{6}$$

The value of the effect atomic number (Z_{eff}) in Eq. (9) was calculated using the value of the atomic cross section (ACS) calculated by Eq. (7) and the effective atomic number (ECS) derived from Eq. (8).

$$ACS = \frac{MAC}{N_A \sum \frac{w}{A}} \tag{7}$$

$$ECS = \frac{1}{N_A}\left(\sum \frac{f \cdot A}{Z} \cdot (MAC)\right) \tag{8}$$

$$Z_{eff} = \frac{ACS}{ECS} \tag{9}$$

where w, f, Z, A are the weight fraction of the element, the fraction of abundance of the element, the atomic number of the element, and the atomic weight of a constituent element, respectively.

Then, the percentage of relative difference (RD) of the results obtained from software Phy-X and XCom was calculated using Eq. (10).

$$RD = \frac{MAC_{XCom} - MAC_{Phy-x}}{MAC_{XCom} + MAC_{Phy-x}} \times 100 \tag{10}$$

Here, MAC_{XCom} stands for the MAC result obtained from software XCom and MAC_{Phy-x} refers to the MAC results obtained from software Phy-X.

2.5 Optical Properties Measurements

Optical absorbance spectrum of glass samples was measured in the wavelength range of 200 to 1100 nm using ultraviolet-visible (UV-VIS) spectrophotometer UV-3600i Plus from Shimadzu. The absorbance (A) values were used to calculate the absorption coefficient (α) using the following Eq. (10).

$$\alpha = 2.303\ \frac{A}{t} \tag{11}$$

where t indicates the thickness of glass samples.

Tauc's plot, a graph of $(\alpha h\nu)^{1/2}$ vs ($h\nu$) was then used to determine the value of E_{opt} where the E_{opt} value can be determined by the x-intercept of the Tauc's plot. Then, to determine the value of molar polarizability (α_m) as shown in Eq. (13) refractive index (n) and molar refraction (R_m) value was calculated using Eq. (11), and Eq. (12), respectively.

$$n = \sqrt{-2 + \frac{3}{\sqrt{\frac{E_{opt}}{20}}}} \tag{12}$$

$$R_m = V_m \left(\frac{n^2-1}{n^2+2}\right) \quad (13)$$

$$\alpha_m = \frac{3}{4}\left(\frac{R_m}{\pi N_A}\right) \quad (14)$$

where π stands for the value of pi, and N_A refers to Avogadro's constant.

3. Results and Discussions

3.1 Glass Composition, Density, and Molar Volume

Figure 1 shows the fabricated glass samples and ceramic samples. The fabrication of the glass samples was stopped at 0.10Bi glass since further incorporation of Bi_2O_3 caused the samples to turn opaque. The opaque nature of 0.15Bi and 0.20Bi ceramics was due to their compact structure which resulted from the excessive incorporation of high-density Bi_2O_3. This caused UV and infrared light unable to transmit through the material causing the material to appear opaque. As for 0.05Bi and 0.10Bi glass, visible light waves were able to transmit through the glass leading to transparent glass. Then, the observed yellowish color of the glass samples is due to the incorporation of Tm_2O_3. The formation of defects in the glass network caused the formation of color centers. These color centers caused glass to absorb and emit specific wavelengths of light [23]. Thulium has an emission wavelength at peaks 458nm, 470 nm, and 650nm where energy transition $^1D_2$ to $^3F_4$, $^1G_4$ to $^3H_6$, and $^1G_4$ to $^3F_4$, respectively occur [24]. This thulium emission wavelength correlates with yellow color emission wavelength which is in the range of 500nm to 650nm [25]. This proved the influence of thulium which caused the visible yellow color of the glass.

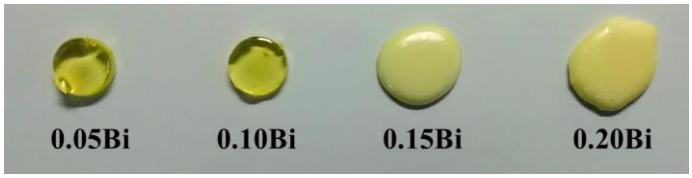

Fig. 1. Fabricated thulium doped bismuth tellurite glass and ceramics

Table 1 summarizes the fabricated samples' chemical composition, molar mass, density, molar volume, oxygen packing density (OPD) and color of fabricated samples. The molar mass of the samples increases as the mol % of Bi_2O_3 incorporated increases. This is due to heavy metal bismuth (Bi) atoms that replace other lighter atoms. Also, the density of the samples increases as the mol % of Bi_2O_3 incorporated increases indicating that a stronger glass network connectivity was formed [26]. Theoretically, the relationship between density and molar volume should be inversely proportional as shown in Eq. (2). However, the molar volume of the fabricated glass increases as the density increases. This indicates the number of non-bridging oxygens (NBOs) reduces in the glass network. The reduction of NBOs was confirmed further by the calculation of OPD. It was found that the OPD increases as the mol % of Bi_2O_3 increases indicating Bi_2O_3 acts as a network former. However, when Bi_2O_3 was added excessively in 0.15Bi and 0.20Bi, the samples turned opaque as shown in Figure 1. When there is too much network in the glass structure, it could block visible light. Thus, only 0.05Bi and 0.10Bi will be characterized further for transparent radiation shielding glass for medical and industrial applications.

Table 1
Sample code, chemical composition, molar mass, density, molar volume, oxygen packing density and color of thulium doped tellurite glass

Sample Code	Chemical Composition (mol %)			Molar Mass (g/mol)	Density (g/cm^3)	Molar Volume (cm^3/g)	Oxygen Packing Density (g/cm^3)	Color
	TeO_2	Bi_2O_3	Tm_2O_3					
0.05Bi	93	5	2	179.44	5.45	32.998	62.731	Transparent Light-yellow
0.10Bi	88	10	2	194.76	5.91	32.938	64.364	Transparent Light- yellow
0.15Bi	83	15	2	210.08	6.41	32.789	66.181	Opaque yellow
0.20Bi	78	20	2	225.40	6.55	34.422	64.493	Opaque yellow

A comparison between the density of fabricated glass samples with lead-based radiation shielding material is shown in Table 2. It is clearly shown that the fabricated glass samples have much higher density than lead glass. This proves the applicability of the glass to be used in industry.

Table 2
Glass code, chemical composition, density, and molar volume of thulium doped tellurite glass

Glass	Density (g/cm^3)
0.05Bi (This work)	5.45
0.10Bi (This Work)	5.91
$(Li_2O_3)_{10}$ $(PbO)_{30}$ $(Bi_2O_3)_{10}$ $(B_2O_3)_{50}$ [27]	4.93
$(Li_2O_3)_{10}$ $(PbO)_{30}$ $(B_2O_3)_{60}$ [27]	4.38
$(Na_2O)_{10}$ $(Quartz)_{60}$ $(PbO)_{30}$ [28]	4.70
RS 323 G19 Schott Glass (33% lead) [29]	3.26
RS 360 Schott Glass (45% lead) [29]	3.60
RS 520 Schott Glass (71% lead) [29]	5.18

3.2 Structural Properties

FTIR analysis was conducted to evaluate the structural bonds that are present in the fabricated thulium-doped bismuth tellurite glass. Figure 2 shows the FTIR spectrum and Table 3 describes the assignment of transmission peaks observed at specific wavenumber. The appearance of the transmittance peak at 622 cm^{-1} wavenumber indicates the stretching vibration of stretching vibrations of TeO_4 structural units [30]. Meanwhile, the presence of Te-O bonds of TeO_3 structural units is indicated by the transmittance peak at 704 cm^{-1} [31,32]. This shows that tellurite is made of TeO_n where n = 4, 3+1, and 3 [33]. The variation of structural units is due to local inhomogeneity whereby electrons do not transfer the glass modifier atoms to all the structural units [34]. In this case, the modifier atoms are Bi. Hence, in the fabricated glass consists of three states of tellurite structural units. However, the structural bonds of Bi-O cannot be observed due to instrument limitations where high noise was observed at a wavenumber lower than 600 cm^{-1} [35]. The Bi-O bonds should be observed at wavenumber 50 cm^{-1} to 500 cm^{-1}. Furthermore, the presence of a sharp peak at 1214 cm^{-1} indicates the bending of water molecules H_2O or/and the overtone of O–Te–O symmetric stretch [36]. Then, the sharp peaks at 1368 cm^{-1} and 1740 cm^{-1} were attributed to the stretching mode of weak Te–OH and strong Te–OH structural bonds. Notice that the intensity of the peaks at wavenumbers 1214 cm^{-1}, 1368 cm^{-1} and 1740 cm^{-1} appear shaper in 0.05Bi glass than 0.10Bi glass. This indicates the incorporation of a glass modifier which in this case Bi_2O_3 reduces the weak hydrogen bonds of Te-OH [36]. Then, the presence of small peaks at 2076 cm^{-1} and 2286 cm^{-1} was due to O-H bond bending while a small peak at 3000 cm^{-1} was due to O-H bond stretching. These O-

H bond bending and stretching were assigned to water molecules type 1 H_2O(I) which were probably trapped in the glass network with restricted motion [37,38]. Based on the FTIR result, the peak for a Tm-O bond was not observed. The peak could not be detected since the concentration of Tm_2O_3 incorporated in the glass composition was very low. A similar result was also observed by Hasnimulyati *et al.,* [39]. However, the presence of thulium can be verified by colour centre as discussed in section 3.1.

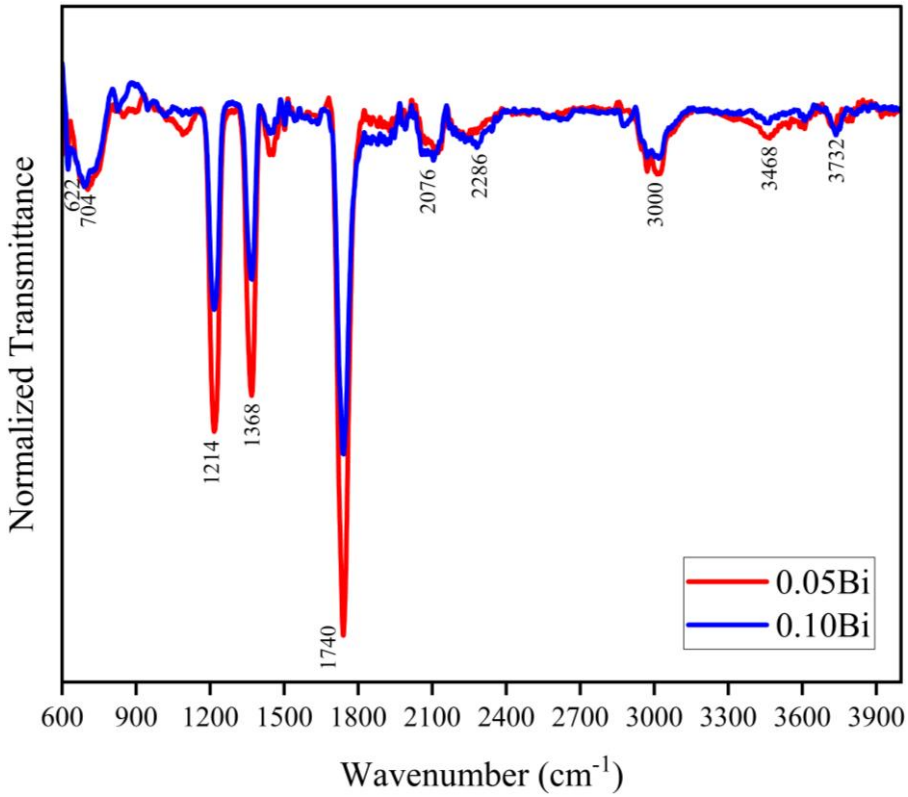

Fig. 2. FTIR spectrum of thulium doped bismuth tellurite glass

Table 3
FTIR structural properties investigation of thulium doped tellurite glass

Wavenumber (cm^{-1})	Assignment	Ref.
622	Stretching vibrations of TeO_4 structural units	Gupta *et al.,* [30]
704	Stretching vibrations of TeO_3/ TeO_{3+1} structural units	Kaur *et al.,* [31] He *et al.,* [32]
1214	Overtone of O–Te–O symmetric stretch and/or bending mode of molecular water	Cheng *et al.,* [36]
1368	Weak Te–OH bonds stretching	Cheng *et al.,* [36]
1740	Strong Te–OH bonds stretching	Cheng *et al.,* [36]
2076	O-H bonds bending vibration of water molecules in glasses	Brokmann *et al.,* [37]
2286		
3000	O-H stretching of water molecule in glasses	Brokmann *et al.,* [37]

3.3 Radiation Shielding Properties

The interaction of photons and radiation shielding material can be observed based on the result of the mass attenuation coefficient (MAC). Based on Figure 3 MAC showed dependency on photon energy where photon interactions such as the photoelectric effect, Compton scattering and pair-production occurred within the attenuated glass. As shown in Figure 3(a) and Figure 3(b), at low

energy levels (0.001 MeV to 0.004 MeV), rapidly decreased of MAC was due to the interaction of the photoelectric effect became dominant [40]. Then, at the intermediate energy level where 0.004 MeV to 0.013 MeV for software XCom in Figure 2(a) and 0.004 MeV to 0.015 MeV for software Phy-X in Figure 2(b), the slower decrease of MAC was due to the interaction of Compton scattering [41]. At high energy which is above 0.013 MeV for software XCom and 0.015 MeV for software Phy-X, the MAC is an almost constant curve indicating the pair production interaction of photons [42].

Based on the result of MAC obtained from software XCom, a few sudden sharp peaks are observed in Figure 3(a). These sharp peaks are due to the absorption edge phenomena. The absorption edge phenomena occur when the absorbed photon energy corresponds to the electronic transition or ionization potential of atoms. The absorption edge peak indication was obtained directly from the software XCom. The Te atoms caused a sudden peak at 1.006×10^{-3} MeV due to the M-absorption edge. Meanwhile, the sharp peaks at 1.515×10^{-3} MeV, 1.850×10^{-3} MeV, and 1.445×10^{-3} MeV were caused by the M-absorption edge of Tm atoms. Then, a peak at 2.668×10^{-3} MeV was attributed to the M-absorption edge of Bi atoms. Three distinguished peaks at 4.341×10^{-3} MeV, 4.612×10^{-3} MeV, and 5.000×10^{-3} MeV were due to the L-absorption edge of Te atoms. However, as for MAC results obtained from software Phy-X in Figure 3(b), the only distinguishable sharp peak only observed at 5.000×10^{-3} MeV. This sharp peak was due to the L-absorption edge of Te atoms.

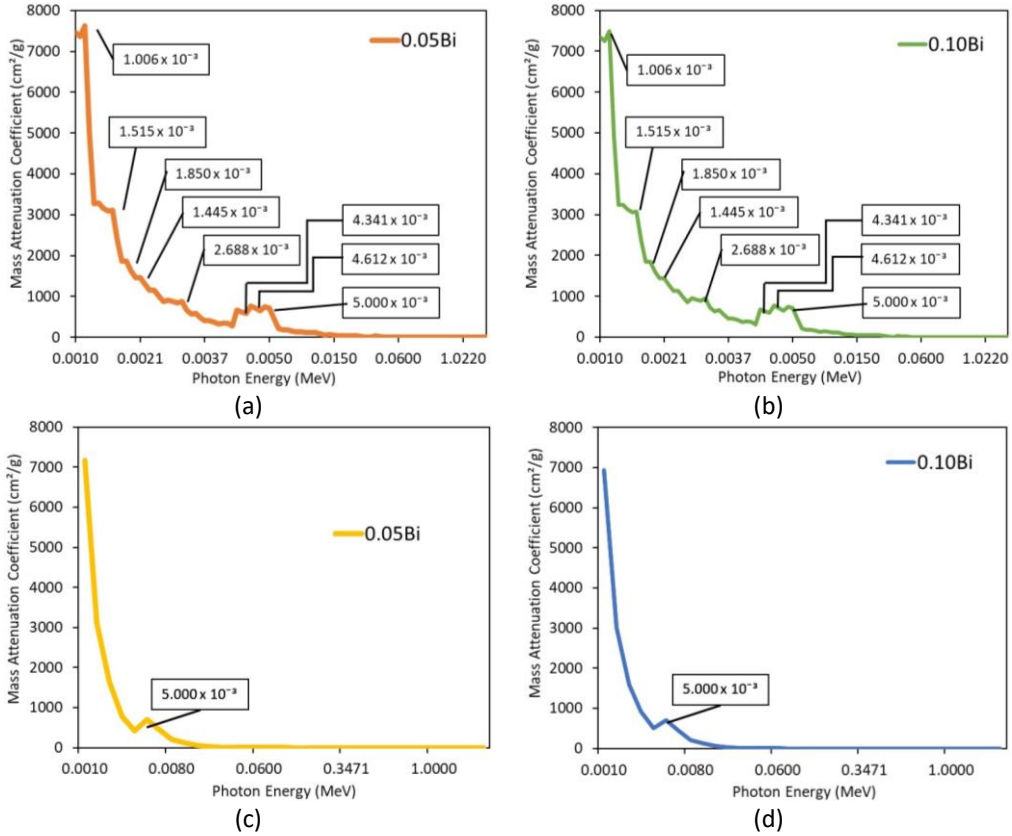

Fig. 3. Mass attenuation coefficient of thulium doped bismuth tellurite glass at different photon energies obtained from software (a) XCom for 0.05Bi glass, (b) XCom for 0.10Bi glass, (c) Phy-X for 0.05Bi glass, and Phy-X for 0.10Bi glass

The percentage of relative difference (RD) of MAC for software Phy-X and XCom is 1.93% for 0.05Bi glass and 3.08% for 0.10Bi glass as shown in Table 4. This low RD indicates that good detection system of the software [43]. The percentage difference was due to systematic error where a different

method was applied for stoichiometric calculation. For software Phy-X, the density of the glasses used for simulation was obtained through an experimental method while software XCom calculated the density of the glass samples based on the molar mass and molar volume of the atoms in the compound mixture.

Table 4
Glass code, mass attenuation coefficient and percentage relative difference of thulium doped bismuth tellurite glass

Glass Code	Mass attenuation coefficient at 0.662 MeV (cm^2/g)		Percentage of relative difference, RD (%)
	Phy-X	XCom	
0.05Bi	0.0801	0.0771	1.93
0.10Bi	0.0838	0.0788	3.08

The half-value layer (HVL) of 0.05Bi and 0.10Bi glass was analyzed at photon energy 0.662 MeV. Photon energy released at 0.662 MeV by ^{137}Cs produced high-energy gamma radiation. This high-energy gamma radiation is currently used in the medical industry especially for cancer treatment as deep tissue penetration can be achieved [44]. Based on the results HVL obtained from software Phy-X and XCom in Figure 4, it was found that the glass with 0.10Bi had lower HVL than 0.05Bi. Low HVL indicates that the material can shield radiation better since the low distance it takes for the harmful radiation rays to reduce to half of its original value.

Figure 5 shows the result of the mean free path (MFP) at a photon energy of 0.662 MeV for software Phy-X and XCom. The MFP indicates the average distance a unit of radiation can travel in the material before being absorbed. The result depicted that the 0.10Bi glass has a lower MFP than 0.05Bi. This low value of MFP in 0.10Bi glass indicates that 0.10Bi glass is more efficient at absorbing radiation rays than 0.05Bi glass [45]. A higher concentration of than Bi_2O_3 in 0.10Bi that 0.05Bi resulted in more photon interaction with radiation shielding glass.

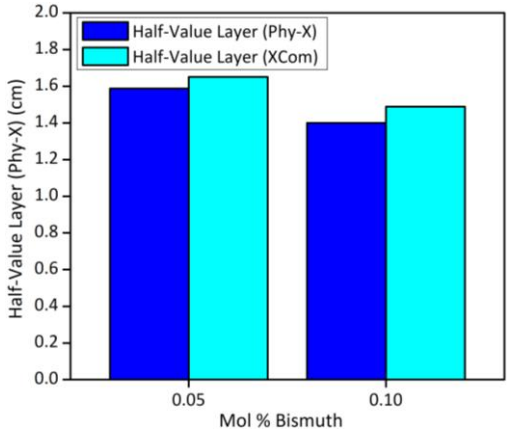

Fig. 4. Half-value layer of thulium doped bismuth tellurite glass at photon energy 0.662 MeV for software Phy-X and XCom

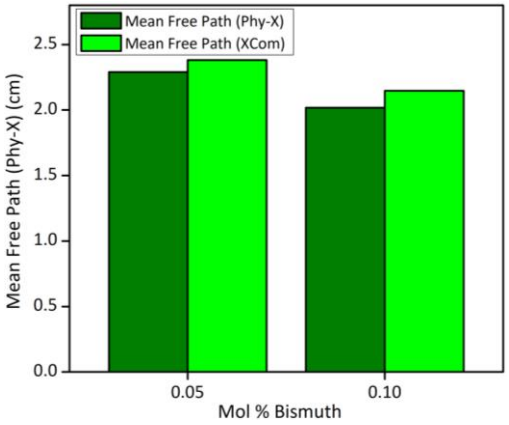

Fig. 5. Mean free path of thulium doped bismuth tellurite glass at photon energy 0.662 MeV for software Phy-X and XCom

Figure 6 shows the result of the effective atomic number (Z_{eff}) of thulium-doped bismuth tellurite glass. The Z_{eff} investigation was conducted at continuous energy between 0.001 MeV to 10 000 MeV, and specifically at 0.662 MeV as shown in Figure 6(a), and Figure 6(b), respectively. Significantly, the Z_{eff} results calculated from software XCom are energy independent while the results simulated from software Phy-X are energy dependent as shown in Figure 6(a). The energy-independent Z_{eff} from software XCom is close to the calculated value of the composition's mean

atomic number. Similar energy-independent Z_{eff} was also observed in a study done by Huse *et al.,* [46]. Hence, this shows the limitation of XCom software. Conversely, the energy-dependent Z_{eff} obtained from software Phy-X makes it possible to evaluate the photon interaction with shielding material.

Similar to MAC, a sharp increase of Z_{eff} at low energy levels was due to the dominant interaction of the photoelectric effect [47]. Meanwhile, a progressive decrease of Z_{eff} at intermediate energy levels indicates Compton scattering becomes dominant [48]. Then, at high energy levels, pair-production interaction dominancy can be portrayed by constant Z_{eff} curves [49]. It is also observed that there are a few sudden sharp peaks in Z_{eff} curves due to the absorption edge. A detailed explanation regarding absorption edge was discussed in the MAC section. Then, the effect of Bi_2O_3 on Z_{eff} at 0.662 MeV photon energy is shown in Figure 6(b). A high value of Z_{eff} is favourable since it indicates that a high number of photons attenuated because shielding material has become the preferred target for photons. Thus, photons would collide more frequently with the atoms of shielding material [11]. The 0.10Bi glass results in a higher value of Z_{eff} at 0.662 MeV photon energy. This is due to the incorporation of bismuth which has a high atomic number causing a high Z_{eff} value. Bismuth which is a heavy element causes more collision of radiation rays to occur within the glass material [50].

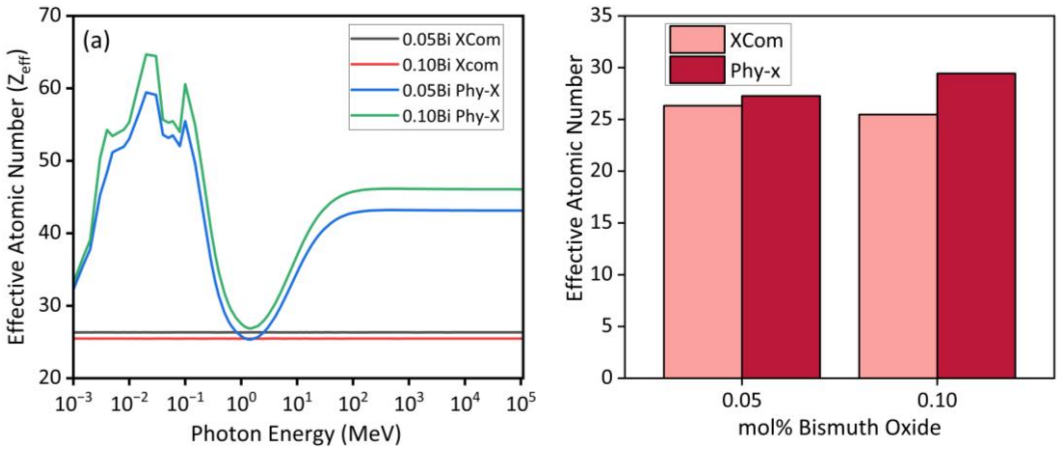

(a) (b)

Fig. 6. Effective atomic number of thulium doped bismuth tellurite glass at (a) continuous energy range from 0.001 MeV to 10 000 MeV, and (b) photon energy 0.662 MeV for software Phy-X and XCom

3.4 Optical Properties

Figure 7 shows the UV-VIS absorption spectra of 0.05Bi and 0.10Bi glass where the investigated wavelength range is 200 nm to 1100 nm. A dominant central wavelength (λ_c) was observed at 321.5 nm for both 0.05Bi and 0.10Bi glass. This central wavelength lies in the visible light spectrum. Based on Figure 7, the absorbed light is higher in 0.10Bi glass than 0.05Bi glass indicating the degree of transparency in 0.10Bi glass is lower than 0.05Bi glass [51]. Then, extrapolation of the graph $(\alpha h\nu)^{1/2}$ vs $(h\nu)$ provides the result of optical band gap (E_{opt}) for 0.05Bi and 0.10Bi glass as shown in Figure 8. The E_{opt} of 0.10Bi glass is higher than 0.05Bi glass due to lower number of NBOs in the glass structure which was proven by OPD. The lower NBO number was caused by the incorporation of Bi_2O_3 in the glass composition resulting in Te–O–Te or O–Te–O bond bending vibrations drastically decreasing in the FTIR spectrum. This results in a more compact structure that was discussed previously in the density section. Both fabricated glasses also exhibit high transparency which is evidenced by the drop

of $(\alpha h\nu)^{1/2}$ vs $(h\nu)$ curves at energies less than E_{opt} [52]. Comparing 0.05Bi and 0.10Bi, the curve of $(\alpha h\nu)^{1/2}$ vs $(h\nu)$ for 0.05Bi drops more drastically than 0.10Bi at energies less than E_{opt}. A drastic drop of $(\alpha h\nu)^{1/2}$ vs $(h\nu)$ indicates a material has high transparency [53].

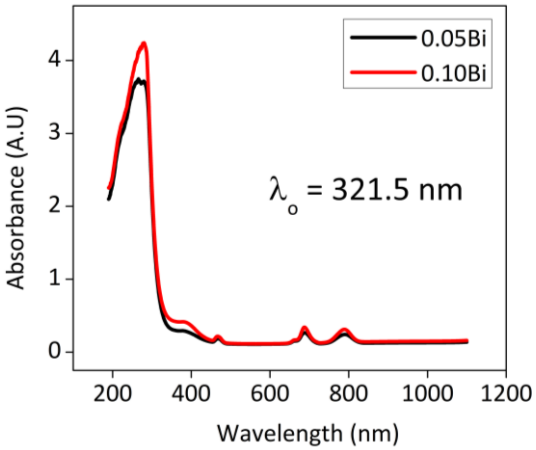

Fig. 7. Absorbance spectra of thulium doped bismuth tellurite glass

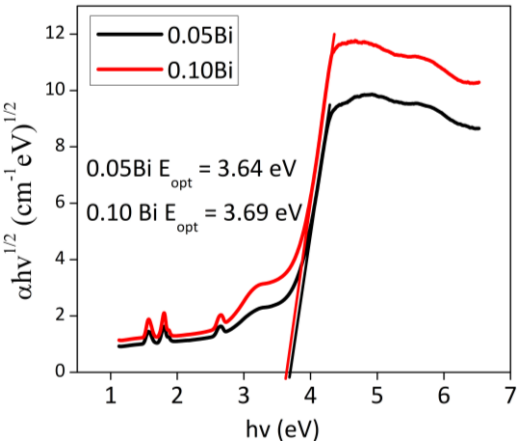

Fig. 8. Tauc's plot graph of $(\alpha h\nu)^{1/2}$ vs $(h\nu)$ for thulium doped bismuth tellurite glass

Figure 9 shows the molar polarizability of 0.05Bi and 0.10Bi glass. The 0.05Bi glass poses slightly higher molar polarizability compared to 0.10Bi. A high number of NBOs caused molar polarizability to also become high [54]. Compared to bridging oxygens (BOs), nonbridging oxygens (NBOs) have a higher tendency to polarize [55]. In applications that require line-of-sight, polarized glass is desired. Polarized glass could eliminate glare which could partially block humans' vision [56]. When polarized sunglasses were applied in road sports, it was found that polarized sunglasses were able to block glare from direct sunlight and sunlight reflected by the road [57].

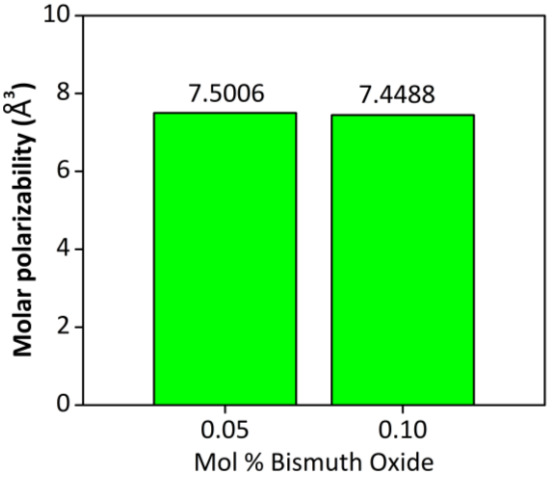

Fig. 9. Bar graph of molar polarizability thulium doped bismuth tellurite glass

4. Conclusions

In this study, a new composition of $TeO_2)_{1-x}$ $(Bi_2O_3)_x$ $(Tm_2O_3)_{0.02}$ was successfully fabricated. Structural investigation by FTIR shows the Te–O–Te or O–Te–O bond bending vibrations and Bi-O bonds. Then, a radiation shielding investigation was conducted using the software Phy-X and XCom. Based on the MAC results, the interaction of the photoelectric effect, Compton scattering, and pair-

production occur at the same energy range for both glasses due to similar compounds incorporated in the glass composition. The 0.10Bi glass exhibits better radiation shielding capability than 0.05Bi glass. This can be seen based on the result of HVL, MFP, and Z_{eff}. The 0.10Bi glass has lower HVL and MFP as well as higher Z_{eff} than 0.05Bi glass. However, in terms of optical properties, the 0.05Bi glass performs better than the 0.10Bi glass. This can be depicted based on the result of absorption spectra, E_{opt} and molar polarizability. The E_{opt} of the 0.05Bi glass is lower than the 0.10Bi glass due to the high number of NBOs in the glass structure which was proven by the low value of OPD. Also, the 0.05Bi glass poses slightly higher molar polarizability compared to 0.10Bi. In applications that require line-of-sight, polarized glass is able to eliminate glare which could partially block humans' vision. All in all, both 0.05Bi and 0.10Bi have higher density than the glass containing lead. Therefore, the fabricated glass sample would perform better as radiation-shielding glass compared to lead glass. Hence, this lead-free glass can be widely used in radiation shielding applications that require transparency.

Acknowledgement
This research was funded by MyBrainSc scholarship and GPJP grant (UPNM/2022/GPJP/SG/3).

References

[1] Dai, Tangye, and Qun Dai. "Effect of blood lead levels on periodontitis in American adults: a cross-sectional analysis from the national health and nutrition examination survey." *BMC Oral Health* 24, no. 1 (2024): 364. https://doi.org/10.1186/s12903-024-04068-1

[2] Green, Rhys E., and Deborah J. Pain. "Partitioning Human Dietary Exposure to Ammunition-Derived Lead in Meat from Game Animals Between Bullets and Shotgun Pellets." *Exposure and Health* (2024): 1-10. https://doi.org/10.1007/s12403-024-00635-7

[3] Wei, Yi-fei, Cui-liu Gan, Fang Xu, Yuan-yuan Fang, Bao-dan Zhang, Wu-shu Li, Kang Nong, Michael Aschner, and Yue-ming Jiang. "Clinical case analysis of 32 children aged 0-6 years with lead poisoning in Nanning, China." *Toxicology and Industrial Health* 40, no. 1-2 (2024): 41-51. https://doi.org/10.1177/07482337231215411

[4] Hydeskov, Helle B., Jon M. Arnemo, Chris Lloyd Mills, Louise K. Gentle, and Antonio Uzal. "A Global Systematic Review of Lead (Pb) Exposure and its Health Effects in Wild Mammals." *The Journal of Wildlife Diseases* 60, no. 2 (2024): 285-297. https://doi.org/10.7589/JWD-D-23-00055

[5] Ilyas, Muhammad Zahaib, Kyu Jin Sa, Muhammad Waqas Ali, and Ju Kyong Lee. "Toxic effects of lead on plants: integrating multi-omics with bioinformatics to develop Pb-tolerant crops." *Planta* 259, no. 1 (2024): 18. https://doi.org/10.1007/s00425-023-04296-9

[6] Ge, Wenjie, Haishen Ren, Yi Zhang, Fei He, Shaohu Jiang, Xiangyu Zhao, and Huixing Lin. "Investigation of the glass forming regularity and thermal behavior of lead-free V_2O_5-TeO_2-RO (R= Ca, Sr, Ba) low temperature sealing glass for electronics packaging." *Journal of Alloys and Compounds* 971 (2024): 172561. https://doi.org/10.1016/j.jallcom.2023.172561

[7] Zubair, Muhammad, Eslam Ahmed, and Donny Hartanto. "Comparison of different glass materials to protect the operators from gamma-rays in the PET using MCNP code." *Radiation Physics and Chemistry* 190 (2022): 109818. https://doi.org/10.1016/j.radphyschem.2021.109818

[8] Li, Kai, Wenchao Zhang, Luyue Niu, Ying Ye, Jing Ren, and Chao Liu. "Lead-free cesium manganese halide nanocrystals embedded glasses for X-ray imaging." *Advanced Science* 10, no. 4 (2023): 2204843. https://doi.org/10.1002/advs.202204843

[9] Díaz Rodríguez, Luis Antonio, Marta Suárez Menéndez, Jose Florindo Bartolomé, Sonia López Esteban, María Belén Cabal Álvarez, Arnaldo Moreno, María del Carmen Bordes, Adolfo Fernández Valdés, Carlos Pecharromán, and José Serafín Moya Corral. "Glass with a low-melting temperature belonging to the P_2O_5-CaO-Na_2O system, applied as a coating on technical ceramics (alumina, zirconia) and traditional ceramics (porcelain stoneware)." *Boletin de la Sociedad Española de Cerámica y Vidrio* (2023). https://doi.org/10.1016/j.bsecv.2023.07.003

[10] Sayyed, M. I. "Radiation Shielding Properties of Aluminosilicate Glass Systems using Phy-X Software." *Journal of Advanced Research in Applied Sciences and Engineering Technology* 37, no. 2 (2024): 156-164. https://doi.org/10.37934/araset.37.2.156164

[11] Rusni, Nur Arina Mat, Hasnimulyati Laoding, and Azuraida Amat. "Theoretical Ionizing Radiation Shielding Parameters of Thulium Doped Zinc Borotellurite Glass." In *E3S Web of Conferences*, vol. 481, p. 03009. EDP Sciences,

2024. https://doi.org/10.1051/e3sconf/202448103009

[12] Shaaban, Kh S., Ali S. Alzahrani, Dalal Abdullah Aloraini, and Yasser A. M. Ismail. "Radiation attenuation and optical behaviors of glass system: $21SiO_2$-$49B_2O_3$-13ZnO-(17-x) Na_2O-xWO_3." *Optical Materials* 148 (2024): 114852. https://doi.org/10.1016/j.optmat.2024.114852

[13] Chen, Yuchang, Ying Shi, Jianjun Xie, Fang Lei, Lingcong Fan, and Lei Zhang. "Fabrication of lead-free low melting temperature TeO_2-V_2O_5-CuO glasses and wetting behavior on AlN ceramic substrate." *Journal of the European Ceramic Society* 40, no. 15 (2020): 5991-6001. https://doi.org/10.1016/j.jeurceramsoc.2020.07.015

[14] Aloraini, Dalal Abdullah, M. I. Sayyed, Ashok Kumar, Sabina Yasmin, Aljawhara H. Almuqrin, D. I. Tishkevich, and A. V. Trukhanov. "Studies of physical, optical, and radiation shielding properties of Bi_2O_3-TeO_2-MgO-Na_2O-B_2O_3 glass system." *Optik* 268 (2022): 169680. https://doi.org/10.1016/j.ijleo.2022.169680

[15] Pious, Aleena, Shreya Muthukumar, Dharshini Karnan Singaravelu, Periyappan Nantheeswaran, Mariappan Mariappan, Arvind Sivasubramanian, Fuad Ameen, Marek Gancarz, and Anbazhagan Veerappan. "Micelle assisted synthesis of bismuth oxide nanoparticles for improved chemocatalytic degradation of toxic Congo red into non-toxic products." *New Journal of Chemistry* 48, no. 1 (2024): 96-104. https://doi.org/10.1039/D3NJ04494G

[16] Wang, Bow, Chien-Yi Ting, Cheng-Shih Lai, and Yi-Shan Tsai. "Bismuth Pelvic X-Ray Shielding Reduces Radiation Dose Exposure in Pediatric Radiography." *BioMed Research International* 2021, no. 1 (2021): 9985714. https://doi.org/10.1155/2021/9985714

[17] Bassam, S. A., K. A. Naseer, Anagha J. Prakash, K. A. Mahmoud, C. S. SuchandSangeeth, M. I. Sayyed, Mohammed S. Alqahtani, E. El Sheikh, and Mayeen Uddin Khandaker. "Effect of Tm_2O_3 addition on the physical, structural, elastic, and radiation-resisting attributes of tellurite-based glasses." *Radiation Physics and Chemistry* 209 (2023): 110988. https://doi.org/10.1016/j.radphyschem.2023.110988

[18] Malidarre, Roya Boodaghi, Iskender Akkurt, Oguz Kocar, and Ismail Ekmekci. "Analysis of radiation shielding, physical and optical qualities of various rare earth dopants on barium tellurite glasses: A comparative study." *Radiation Physics and Chemistry* 207 (2023): 110823. https://doi.org/10.1016/j.radphyschem.2023.110823

[19] Alomayrah, Norah, Z. A. Alrowaili, Norah Salem Alsaiari, H. H. Saleh, S. M. Ibrahim, Izhar Ahmed, Chahkrit Sriwunkum, I. O. Olarinoye, and M. S. Al-Buriahi. "Gamma attenuation properties of Tm_2O_3 doped tellurite glass for radiation shielding." *Journal of Radiation Research and Applied Sciences* 17, no. 3 (2024): 100983. https://doi.org/10.1016/j.jrras.2024.100983

[20] Azuraida, A., O. Nurshahidah, W. Y. W. Yusoff, R. Falihan, N. A. Abdul-Manaf, and N. Ahmad. "Effect of thulium boro-tellurite glass system on radiation shielding parameters." *Journal of Ovonic Research* 18, no. 2 (2022): 141-148. https://doi.org/10.15251/JOR.2022.182.141

[21] Thoraeus, R. "Cesium 137 and its gamma radiation in teleradiotherapy." *Acta Radiologica* 5 (1961): 385-395. https://doi.org/10.3109/00016926109175133

[22] Sayyed, M. I., B. O. El-bashir, Abdullah M. S. Alhuthali, Y. S. M. Alajerami, Y. Al-Hadeethi, and Mohammad Hasan Abu Mhareb. "Gamma radiation shielding and structural features for barium strontium boro-tellurite glass modified with various concentrations of molybdenum oxide." *Journal of Non-Crystalline Solids* 559 (2021): 120658. https://doi.org/10.1016/j.jnoncrysol.2021.120658

[23] Halimah, M. K., L. Hasnimulyati, A. Zakaria, S. A. Halim, M. Ishak, A. Azuraida, and Naif Muhammed Al-Hada. "Influence of gamma radiation on the structural and optical properties of thulium-doped glass." *Materials Science and Engineering: B* 226 (2017): 158-163. https://doi.org/10.1016/j.mseb.2017.09.010

[24] Louot, Christophe, Félix Sanson, Arnaud Motard, Thierry Ibach, Inka Manek-Hönninger, Antoine Berrou, Nicolas Dalloz, Thierry Robin, Benoit Cadier, and Anne Hildenbrand-Dhollande. "Emission Wavelength Limits of a Continuous-Wave Thulium-Doped Fiber Laser Source Operating at 1.94 µm, 2.09 µm or 2.12 µm." In *Photonics*, vol. 11, no. 3, p. 246. MDPI, 2024. https://doi.org/10.3390/photonics11030246

[25] Lanièce, Alexandra. "Alveoli-on-a-chip: a close-contact dynamic model of the alveolar capillary barrier: microengineering, microfluidics and induced pluripotent stem cells| Theses. fr." *PhD diss., Sorbonne Paris Cité*, 2018.

[26] Effendy, Nuraidayani, Sidek Hj Ab Aziz, Halimah Mohamed Kamari, Mohd Hafiz Mohd Zaid, Caceja Elyca Anak Budak, Muhammad Kashfi Shabdin, Mohammad Zulhasif Ahmad Khiri, and Siti Aisyah Abdul Wahab. "Artificial neural network prediction on ultrasonic performance of bismuth-tellurite glass compositions." *Journal of Materials Research and Technology* 9, no. 6 (2020): 14082-14092. https://doi.org/10.1016/j.jmrt.2020.09.107

[27] Saleh, Emran Eisa, Mohammed A. Algradee, S. A. El-Fiki, and G. M. Youssef. "Fabrication of novel lithium lead bismuth borate glasses for nuclear radiation shielding." *Radiation Physics and Chemistry* 193 (2022): 109939. https://doi.org/10.1016/j.radphyschem.2021.109939

[28] Kassem, Said M., G. S. M. Ahmed, A. M. Rashad, S. M. Salem, S. Ebraheem, and A. G. Mostafa. "An investigation of the nuclear shielding effectiveness of some transparent glasses manufactured from natural quartz doped lead cations." *Nuclear Engineering and Technology* 53, no. 6 (2021): 2025-2037.

https://doi.org/10.1016/j.net.2020.12.023
[29] Schott. "Product Variants of Radiation Shielding Glasses." *Schott*, 2024. https://www.schott.com/en-my/products/radiation-shielding-glasses-p1000330/product-variants.
[30] Gupta, Nupur, Atul Khanna, Ann-Christin Dippel, and Olof Gutowski. "Structure of bismuth tellurite and bismuth niobium tellurite glasses and $Bi_2Te_4O_{11}$ anti-glass by high energy X-ray diffraction." *RSC Advances* 10, no. 22 (2020): 13237-13251. https://doi.org/10.1039/D0RA01422B
[31] Kaur, Amandeep, Atul Khanna, Himal Bhatt, Marina Gónzález-Barriuso, Fernando González, Banghao Chen, and M. N. Deo. "BO and TeO speciation in bismuth tellurite and bismuth borotellurite glasses by FTIR, 11B MAS-NMR and Raman spectroscopy." *Journal of Non-Crystalline Solids* 470 (2017): 19-26. https://doi.org/10.1016/j.jnoncrysol.2017.04.028
[32] He, Jianli, Huan Zhan, and Aoxiang Lin. "Structural property of bismuth-doped tellurite glasses for nonlinear and Raman fiber applications." *Optical Materials* 96 (2019): 109280. https://doi.org/10.1016/j.optmat.2019.109280
[33] Jan, N. A. M., and M. R. Sahar. "Effect of heat treatment on the structural modification of neodymium doped tellurite glass." *Chalcogenide Letters* 13, no. 9 (2016): 417-426.
[34] Suehara, Shigeru, Kazuo Yamamoto, Shunichi Hishita, Takashi Aizawa, Satoru Inoue, and Akihiko Nukui. "Bonding nature in tellurite glasses." *Physical Review* B 51, no. 21 (1995): 14919. https://doi.org/10.1103/PhysRevB.51.14919
[35] Szaller, Zs, L. Kovacs, and L. Pöppl. "Comparative study of bismuth tellurites by infrared absorption spectroscopy." *Journal of Solid State Chemistry* 152, no. 2 (2000): 392-396. https://doi.org/10.1006/jssc.2000.8695
[36] Cheng, Yin, Wu Zhongqing, Hu Xi, Wu Tengyan, and Zhou Weiwei. "Thermal stability and optical properties of a novel Tm^{3+} doped fluorotellurite glass." *Journal of Rare Earths* 32, no. 12 (2014): 1154-1161. https://doi.org/10.1016/S1002-0721(14)60197-6
[37] Brokmann, Ulrike, Christoph Weigel, Luisa-Marie Altendorf, Steffen Strehle, and Edda Rädlein. "Wet Chemical and Plasma Etching of Photosensitive Glass." *Solids* 4, no. 3 (2023): 213-234. https://doi.org/10.3390/solids4030014
[38] Uchino, Takashi, Tetsuo Sakka, and Matae Iwasaki. "Interpretation of hydrated states of sodium silicate glasses by infrared and Raman analysis." *Journal of the American Ceramic Society* 74, no. 2 (1991): 306-313. https://doi.org/10.1111/j.1151-2916.1991.tb06880.x
[39] Hasnimulyati, L., M. K. Halimah, A. Zakaria, S. A. Halim, M. Ishak, and C. Eevon. "Structural and optical properties of Tm_2O_3-doped zinc borotellurite glass system." *Journal of Ovonic Research* 12, no. 6 (2016): 291-299.
[40] Azuraida, A., M. K. Halimah, M. Ishak, N. R. Fadhilah, A. Norhayati, and N. Ahmad. "Mass Attenuation Coefficient of $[(TeO_2)_{0.7}(B_2O_3)_{0.3}](BaO)_x$ Glass for Energy of 1 KeV-100 GeV." *Chalcogenide Letters* 18, no. 3 (2021): 123-127. https://doi.org/10.15251/CL.2021.183.123
[41] Saleh, A., Rizk Mostafa Shalaby, and Nermin Ali Abdelhakim. "Comprehensive study on structure, mechanical and nuclear shielding properties of lead free Sn-Zn-Bi alloys as a powerful radiation and neutron shielding material." *Radiation Physics and Chemistry* 195 (2022): 110065. https://doi.org/10.1016/j.radphyschem.2022.110065
[42] Halimah, M. K., A. Azuraida, M. Ishak, and L. Hasnimulyati. "Influence of bismuth oxide on gamma radiation shielding properties of boro-tellurite glass." *Journal of Non-Crystalline Solids* 512 (2019): 140-147. https://doi.org/10.1016/j.jnoncrysol.2019.03.004
[43] Limkitjaroenporn, P., J. Kaewkhao, P. Limsuwan, and W. Chewpraditkul. "Physical, optical, structural and gamma-ray shielding properties of lead sodium borate glasses." *Journal of Physics and Chemistry of Solids* 72, no. 4 (2011): 245-251. https://doi.org/10.1016/j.jpcs.2011.01.007
[44] Russ, Eric, Catherine M. Davis, John E. Slaven, Dmitry T. Bradfield, Reed G. Selwyn, and Regina M. Day. "Comparison of the medical uses and cellular effects of high and low linear energy transfer radiation." *Toxics* 10, no. 10 (2022): 628. https://doi.org/10.3390/toxics10100628
[45] Al-Hadeethi, Yas, Moustafa Ahmed, Saleh H. Al-Heniti, M. I. Sayyed, and Y. S. Rammah. "Rare earth Co-Doped tellurite glass ceramics: Potential use in optical and radiation shielding applications." *Ceramics International* 46, no. 11 (2020): 19198-19208. https://doi.org/10.1016/j.ceramint.2020.04.257
[46] Huse, S. D., S. S. Obaid, A. A. Joshi, D. K. Gaikwad, P. P. Pawar, and A. R. Shitre. "Study on the radiation shielding features of some chemical compounds." In *Journal of Physics: Conference Series*, vol. 1644, no. 1, p. 012061. IOP Publishing, 2020. https://doi.org/10.1088/1742-6596/1644/1/012061
[47] Sayyed, M. I., M. H. A. Mhareb, and M. Kh Hamad. "Physical, Mechanical, and ionizing radiation shielding properties of $10PbO\text{-}10Na_2O\text{-}(80\text{-}x)\ B_2O_3\text{-}xBaO$ glasses." *Optical Materials* 150 (2024): 115237. https://doi.org/10.1016/j.optmat.2024.115237
[48] Mostafa, A. M. A., Shams A. M. Issa, E. F. El Agammy, Hesham M. H. Zakaly, B. M. Alotaibi, and F. Gharghar. "Effect of BaO addition on gamma radiation shielding performance of sodium barium borate glasses using FLUKA code and PhyX/PSD platform." *Radiation Physics and Chemistry* 206 (2023): 110766. https://doi.org/10.1016/j.radphyschem.2023.110766
[49] Ardiansyah, Ardiansyah, Heryanto Heryanto, Bidayatul Armynah, Hassan Salah, Abdelmoneim Sulieman, David A.

Bradley, and Dahlang Tahir. "Physical, mechanical, optical, and gamma radiation shielding properties of the BaO-based glass system prepared by the melt-quench technique: a review." *Radiation Physics and Chemistry* 210 (2023): 111059. https://doi.org/10.1016/j.radphyschem.2023.111059

[50] Al-Buriahi, M. S., M. Rashad, Amani Alalawi, and M. I. Sayyed. "Effect of Bi_2O_3 on mechanical features and radiation shielding properties of boro-tellurite glass system." *Ceramics International* 46, no. 10 (2020): 16452-16458. https://doi.org/10.1016/j.ceramint.2020.03.208

[51] Sayyed, M. I., A. Ibrahim, M. A. Abdo, and M. S. Sadeq. "The combination of high optical transparency and radiation shielding effectiveness of zinc sodium borate glasses by tungsten oxide additions." *Journal of Alloys and Compounds* 904 (2022): 164037. https://doi.org/10.1016/j.jallcom.2022.164037

[52] Zhumekenov, Ayan A., Makhsud I. Saidaminov, Md Azimul Haque, Erkki Alarousu, Smritakshi Phukan Sarmah, Banavoth Murali, Ibrahim Dursun et al. "Formamidinium lead halide perovskite crystals with unprecedented long carrier dynamics and diffusion length." *ACS Energy Letters* 1, no. 1 (2016): 32-37. https://doi.org/10.1021/acsenergylett.6b00002

[53] Mannino, Giovanni, Ioannis Deretzis, Emanuele Smecca, Antonino La Magna, Alessandra Alberti, Davide Ceratti, and David Cahen. "Temperature-dependent optical band gap in $CsPbBr_3$, $MAPbBr_3$, and $FAPbBr_3$ single crystals." *The Journal of Physical Chemistry Letters* 11, no. 7 (2020): 2490-2496. https://doi.org/10.1021/acs.jpclett.0c00295

[54] Halimah, M. K., M. F. Faznny, M. N. Azlan, and H. A. A. Sidek. "Optical basicity and electronic polarizability of zinc borotellurite glass doped La^{3+} ions." *Results in Physics* 7 (2017): 581-589. https://doi.org/10.1016/j.rinp.2017.01.014

[55] Azlan, M. N., M. K. Halimah, S. Z. Shafinas, and W. M. Daud. "Electronic polarizability of zinc borotellurite glass system containing erbium nanoparticles." *Materials Express* 5, no. 3 (2015): 211-218. https://doi.org/10.1166/mex.2015.1236

[56] Lingelbach, Bernd, and Gernot Jendrusch. *Polarizing Filters in Ski Sports*. ASTM International, 2010.https://doi.org/10.1520/JAI102826

[57] Mercatelli, Luca. "Examining polarizing and non-polarizing filters for road sports." *Frontiers in Sports and Active Living* 5 (2023): 1236473. https://doi.org/10.3389/fspor.2023.1236473